EXPERIMENTAL STUDY OF THE EXIT VELOCITY DISTRIBUTION IN A SHORT VORTEX CHAMBER

Bing S. Luh

A DISSERTATION
in
The Faculty
of
Engineering

Presented in partial fulfilment of the requirements for the
Degree of Master of Engineering at
Sir George Williams University
Montreal, Canada

September, 1973

EXPERIMENTAL STUDY OF THE EXIT VELOCITY DISTRIBUTION IN A SHORT VORTEX CHAMBER

ABSTRACT

A 10-inch vortex chamber (with independently controlled tangential and radial flow inlets) had been built. Detailed measurements of the velocity profile at the exit plane of the vortex chamber revealed the existence of a strong reverse axial flow near the chamber axis, and the interdependency of this flow with the tangential input momentum. Radial velocity distribution studies indicated the existence the counter-rotating Taylor-Görtler type vortex rings whose rotating motions are superimposed upon the vortex spiralling flow pattern.

The experimental results provided may yield insights into the complex flow configurations of vortex flows with high swirl conditions. Some of these findings will aid the design of devices based on vortex motions.

ACKNOWLEDGEMENTS

The author wishes to express his appreciation to his supervisors, Dr. C.K. Kwok and Dr. S. Lin, for their guidance and advice throughout the course of this work. The numerous discussions and valuable help given by Dr. R.L. Wang and Mr. P.M. Lee are very much appreciated.

This work was supported by the National Research Council of Canada under grants No. 7435 and No. A7929.

LIST OF FIGURES

The 2.0 Inch Diameter Cylindrical Exhaust Port:

The 1.5 Inch-Diameter Cylindrical Exhaust Port:

The 3.6 Inch-Diameter Conical Exhaust Port:

Figure page

Static Pressure Distribution in 10 Inch Diameter Chamber:

TABLE OF CONTENTS

NOTATIONS

a	cross-sectional area of probe, sq. in.
A	flow area of exhaust port, sq. in.
D_{ex}	exhaust port diameter, in.
P_1	indicated total pressure
P_2, P_3	indicated static pressure
P_4, P_5	pitch angle pressure
P_s	static pressure
P_{s1}	true static pressure
P_t	true total pressure
Q	total flow rate, $ft^3/min.$
Q_c	control flow rate, $ft^3/min.$
Q_s	supply flow rate, $ft^3/min.$
V	velocity, ft/min.
r, ϕ, z	cylindrical coordinate
V_r, V_ϕ, V_z	radial, tangential, and axial velocity components cylindrical coordinate, ft/sec.
θ	pitch angle, degrees
ρ	fluid density, slug/cu.ft.
ψ	yaw angle, degrees
μ	dynamic viscosity, $lb_f\text{-}sec/ft^2$
μ_a	apparent dynamic viscosity

CHAPTER 1

INTRODUCTION

The study of vortex flow phenomena has always been a key subject for research in the field of fluid mechanics. Many practical applications involve the use of vortex flow phenomena, such as in nuclear reactors, gas turbines and chemical industries.

The emergence of fluid logic as an upcoming technology has stimulated the creation of many ingenious ideas and fascinating concepts, many of which have stimulated further interest in applications of confined vortex motion.

In the past thirty years, swirling flow phenomena have been discussed by many authors and analyzed by prominent people in the field of fluid mechanics. Since the early forties, a vast amount of information on the swirling flow phenomena was published attempting to interpret the experimental results obtained from viscous vortex motion by theoretical solutions of the Navier-Stokes equations using either approximate or numerical methods.

The majority of the analytical work in this period attempted to develop a vortex flow model either by assuming an inviscid flow or by using a viscosity equal to that found in a laminar flow. For example, Rott (1) discussed the dissipation of a vortex of infinite extent by assuming radial and axial velocity distributions to find an explicit solution for tangential velocity. Later Donaldson and Sullivan (2) introduced a more general solution for vortex motion applicable, however, only in a laminar region. The Navier-Stokes equations in cylindrical form were solved numerically using boundary conditions applied for the specific problems considered.

Very few articles are available concerning the results of detailed measurements of flow velocity profiles within the vortex chamber. Kendall (3) used an optical method to measure the tangential, axial and radial velocity components by tracking fine aluminum particles at selected positions within a hydraulic cyclone whose vortex motions were generated within a rotating porous ring which induced a swirl to the fluid passing through it. He used a flattened pitot probe to determine flow direction and total pressure. The results indicated that the maximum flow occurred at the measuring station closest to the solid boundary, and gradually decreased when moving away from the wall. A more revealing experimental investigation concerning confined vortex flow was repeated by Kwok (4) who measured not only the wall static pressure distributions of a short vortex chamber of aspect ratio* 0.02, but also conducted detailed measurements of the velocity profile at the exit plane of the central exhaust port. He compared the experimental measurements with his two-cell analytical model and found that strong reverse flow

---

*Aspect ratio is defined as the ratio of the chamber height to its diameter.

existed for confined vortex flow with high swirl, and that the apparent viscosity associated with the flow was of a magnitude several thousand times greater than that for the laminar case.

Savino and Ragsdale (5) made detailed measurements of velocity components and pressure distributions within a particular vortex chamber of aspect ratio 0.5. They used 48 accurately aligned tangential guide vanes to generate the vortex motion in the chamber and used a 3-tube pitot-yaw probe capable of indicating both the pressure and flow direction to accurately determine the velocity components. Beverloo et al. (6) made radial traverses of the total pressure within short vortex chambers of various aspect ratios for a variety of outlet orifices, and tangential injection port configurations. The results provided information on the radial distribution of tangential velocity profiles only.

In the early sixties, experimental work on confined vortex flow was greatly intensified following the 1957 proposal by Kerrebrock and Meghreblian (7) of the cavity reactor concept for nuclear rocket propulsion and their 1959 vortex magnetohydrodynamics power generator (8). Williamson and McCune (9) conducted experimental measurements on a confined vortex chamber of aspect ratio from 0.13 to 0.218. They conducted axial traverses of the total pressure and calculated the radial distribution of tangential velocity based on these measurements.

Williamson and Donaldson (10) made measurements of the tangential and radial velocity components within a cylindrical chamber of aspect ratio 0.167. Air was injected through an outer porous ring and removed through a stationary concentric porous inner cylinder. Yaw probes were used to determine the velocity components. The results indicated that the velocity distributions corresponded quite closely to those found by Kendall (3).

Recently, King (11), Weber (12), Ostrach and Loper (13) have considered the development of the boundary layer on the end wall of a vortex chamber, as a result of the swirl flow. But perhaps the most significant recent contribution is the work of Wormley (14), who performed experimental investigation using a vortex chamber of 7 inch diameter. Various flow patterns were studied for a range of velocity ratios within the vortex chamber. A momentum integral analysis was developed for the incompressible, steady, axisymmetric flow in a short vortex chamber which confirmed the findings of some previous investigators.

In many recently developed devices where vortex motion is utilized, such as the vortex atomizer, vortex amplifiers and vortex meters, jets of fluid are introduced tangentially at the peripheral wall of the circular vortex chamber. This flow resembles flow along concave walls where the destabilizing effects of the centrifugal forces created Taylor-Görtler vortices along the flow path.

The design of such devices is by no means a simple task since, at present, even though hundreds of papers have been published on subjects related to vortex motions, the complex flow mechanism is still not fully understood. Further experimental investigations are needed to acquire a better physical insight into the flow field existing in a confined vortex chamber.

The present investigation was initiated following the findings described by Thinh (15), Wei (16), and Kwok and Lin (17). Thinh (15) developed an analysis of the vortex motion by including the apparent viscosity factor. The numerical solutions were compared with those of existing experimental measurements by Savino (5). The analytical results proved that the values of the apparent viscosity seriously affect the velocity profiles within the vortex chamber. The results also show that the apparent viscosity within the vortex chamber varies from 7000μ at the chamber periphery to 4500μ at the edge of the central exhaust port, where μ is the operating fluid viscosity.

In references (16) and (17), the authors performed measurements of the velocity profiles in the exhaust port of a short cylindrical chamber, and tried to interpret the results from a physical standpoint to achieve a better understanding of the complex flow mechanism.

The aim of the present study is to further extend the measurements described in references (16) and (17) for a variety of exhaust port configurations. Experimental results will be critically analyzed and discussed. The experiments described in this dissertation were performed under similar circumstances to those described in references (16) and (17) and the author is indebted to Wei, Kwok and Lin for their lucid explanations which provided an inspiration for parts of this dissertation. The results will be useful for comparison with the results of future theoretical work on three-dimensional flow in the exhaust port in order to establish the value of apparent viscosity.

CHAPTER 2

EXPERIMENTAL SET-UP AND PROCEDURES

In order to achieve the stated objectives, it was necessary to acquire three major pieces of apparatus:

a) A cylindrical vortex chamber with built-in flexibility for adjustment of aspect ratio and for control of input velocity ratio.

b) A probe capable of measuring the flow velocity at the exhaust port.

c) A traversing mechanism providing a three-dimensional adjustment with linear movement accurate to 0.05 inch.

Each piece of apparatus is described in detail in the following sections.

2.1 The Vortex Chamber

The present investigation utilizes a vortex chamber which was designed by employing a concept similar to that of the vortex amplifier used in fluidic technology. The general configuration of a vortex amplifier can be described as having radial supply flow inlets and tangential flow inlets. The flow through these inlets is referred to as the power flow, and control flow respectively. The supply or power flow enters behind a circular plate and then passes around the plate into the vortex chamber as shown in Fig. 1.

This configuration forces the supply flow to enter the vortex chamber through an annular gap. The control flow issues from tangentially aligned jets introduced into the annulus at right angles to the radial flow. When mixing of the two flows takes place, swirl is imparted to the supply flow by the tangential velocity of the control jets in the annulus.

The 10 inch diameter vortex chamber used in the study has a total of eight identical tangential nozzles, each 0.219 inch in diameter, symmetrically placed along the periphery of the chamber. The intensity of swirl is governed by the strength of the control jets which in turn is determined by the pressure in the control jet plenum chamber. Flow is discharged into the atmosphere through a central exhaust port. The exhaust port is designed to facilitate installation of various sizes and shapes of outlet as shown in Fig. 2. There are three interchangeable outlet ports, two of which are cylindrical with inside diameters of 1.5 and 2.0 inches. The third exhaust port has an exit hole diameter of 3.6 inches with an included angle of 30°. Interchangeable chamber spacers are made to allow the adjustment of the vortex chamber height from 0.0 to 1.625 inches. In other words, experimental measurements may be conducted on a vortex chamber of aspect ratios from 0.0 up to 0.1625.

The end wall on the side of the outlet port was fabricated with a total of 22 wall static pressure taps at various radial positions. All the pressure taps were 0.0625 inch in diameter, and were carefully machined with clean square edges to ensure validity of the experimentally measured pressure values.

2.2 Directional Probe

The major objective of this experimental study is to measure accurately the velocity profiles at the exit plane of the vortex exhaust core region. The flow leaving the vortex chamber, as may be expected, is highly complex in nature. Therefore, in order to obtain the correct velocity vector, the flow direction at any point must first be determined carefully.

In this study, it was decided to use a five-hole 3-dimensional probe, model DA125, produced by United Sensor and Control Corp. This probe has a five-hole, prism-shaped measuring section and is capable of measuring yaw and pitch angles, static and total pressures accurately within the range stated by the manufacturer.

2.3 Traversing Mechanism

The traversing mechanism used was designed previously for use in turbulent flow measurements (shown in Fig. 3). The main traversing system permits movement in three dimensions with an accuracy of 0.05 inch. A separate unit, mounted on the "z" traverse axis, has a probe-holder capable of additional three-dimensional movement for space correlations. The accuracy of this unit is approximately 0.0005 inch. An adjustable disc dial is fitted to the tip of the probe-holder which can be rotated in the horizontal or vertical plane. Accuracy of the angular calibration of the dial is within two degrees.

2.4 Test Procedure

On the two-inch diameter cylindrical exhaust port, 11 sets of experiments were carried out covering supply flow rates of 10, 20 and 30 scfm, and control flow rates of 5, 10 15 and 20 scfm. For a typical run, the supply and control flow rates were adjusted to the desired values. Error in flowmeter readings due to back pressure effects were corrected using the manufacturer's recommended procedure. For the 1.5-inch diameter cylindrical exhaust port, eight sets of results were obtained covering supply flow rates of 10, 20 and 30 scfm, and control flow rates of 5, 7, 10 and 15 scfm. For the 3.6 inch exit diameter conical exhaust port, there are nine sets of results with supply flow rates ranging from 10 to 30 scfm and control flow rates from 10 to 20 scfm. All these results were obtained using the 10-inch diameter chamber with an aspect ratio of 0.05 inch.

Since it takes time for flow to reach its steady state with each change of the test conditions, special precautions were taken so that at least five minutes elapsed to allow the flow, as well as the manometers, to reach steady state values. The wall static pressure was measured by water manometers. Airflow Development Ltd. liquid-filled inclined manometers using special liquid of S.G. = 0.787 were used to measure the pressure of the five-hole probe. These manometers were readable to within 0.05 inch accuracy. The probe was first aligned in a horizontal plane by means of a transit and later place 0.0625 inch away from the exit plane of the exhaust port. The probe was then rotated until the pressure difference between the two yaw pick-off tubes was zero. The yaw angle "ψ" of the flow velocity vector at the measuring point was then indicated on the dial of the traversing mechanism.

All the pressures, P_1, P_2, P_3, P_4 and P_5, from the five-hole directional probe, as shown in Fig. 4, were recorded. Pitch angle "θ" was determined by calculating $[(P_4-P_5)/(P_1-P_2)]$ and using the calibration curves of the probe supplied by the manufacturer. Once the pitch angle was known, the velocity pressure coefficient $[(P_t-P_s)/(P_1-P_2)]$, and total pressure coefficient $[(P_1-P_t)/(P_t-P_s)]$, could be read directly from other calibration curves supplied by the manufacturer of the probe. P_t and P_s are the total and static pressures respectively. With the velocity pressure and total pressure coefficients known, P_t, P_s, and (P_t-P_s) could be calculated.

The static pressure P_s found in this manner is subject to error. When a probe is introduced into the flow, the cross-sectional area of the flow is reduced and static pressure changes. In other words, the static pressure P_s derived from the measured values will not be the same as the true static pressure, P_{s1}. When this type of probe is placed in the flow, the actual drop in static pressure at the probe cross-section and downstream from it is approximately*: $(P_{s1}-P_s)/(P_t-P_{s1}) = 1.2\ a/A$, where a/A is the fraction of passage area A blocked by the cross-sectional area of probe a. Since P_s, P_t, A and a were all known, the true static pressure, P_{s1}, was found from the last equation. As soon as the corrected total pressure P_t, static pressure P_{s1}, yaw and pitch angles (ψ,θ) were known, the velocity and velocity components were determined by means of Bernoulli's equation. The detailed data reduction is shown in Appendix I. The vector diagram in cylindrical coordinates is shown in Fig. 5.

---

*This expression for correction was recommended by United Sensor Corp., manufacturer of the 5-hole directional probe.

CHAPTER 3

ANALYSIS OF RESULTS

3.1 Presentation of Test Data

A number of tests were conducted on the experimental vortex chamber described in Section 2.1. Tests covered ranges of supply flow rates, "Q_s", of 10, 20 and 30 scfm. Unlike in references (16) and (17), where only one two inch diameter exhaust port was used, this experimental investigation covers three different exhaust port configurations, two cylindrical and one 30° conical, with exit diameters of 1.5, 2.0 and 3.6 inches respectively.

Detailed experimental data of velocity profiles are presented in Figs. 6 to 14 covering cases of all three different exhaust ports. Although for each geometric configuration data on tangential, radial and axial velocity components are presented together for constant supply flow rate and varying control flow rates, discussion will be carried out on the radial distribution of each velocity component separately. It must be understood that the term "control flow" does not carry the same connotation as in the vortex amplifier. The control flow in this context represents the magnitude of the angular momentum imparted to the vortex flow.

Wall static pressure distributions were recorded for different test runs and are presented in Figs. 15, 16 and 17. These pressure readings represent pressures in the annular region before flow entered the central exhaust port. Because of the strategic location of these pressure taps described in reference (16), it is possible to check the flow symmetry as well as recognize the general trend of the pressure drop across the vortex chamber.

3.2 Radial Distribution of Axial Velocity Component

3.2.1 The 2 inch diameter cylindrical exhaust port

The results of the radial distribution of axial velocity components for a constant supply flow rate of 10, 20 and 30 scfm and values of control flow rates of 5, 10, 15 and 20 scfm for the two inch diameter exhaust port are presented in Figs. 6b, 7b and 8b. There are certain common features in these curves. First, they all indicate positive (outward) maximum flow near the edge of the exhaust port and negative (reverse) flow near the centre. The magnitudes of the outward and reverse flow are very much dependent on the control flow. It may be explained that as the control flow is increased, the tangential momentum imparted to the flow is also increased. According to the principle of conservation of momentum, the tangential velocity component is bound to increase as the flow spirals its way towards the centre. The increase in velocity will result in a decrease in static pressure which eventually will reach a level below that of the ambient. At this moment, the ambient air will be sucked into the flow. This is indicated by the experimental results shown in Figs. 6b, 7b and 8b. For higher control flow rates, the magnitude of the tangential velocity near the centre is also increased and the drop in static pressure is correspondingly intensified. This is substantiated by the fact that both the outward and reversed axial velocity components are increased with increasing control flow.

As the axial velocity component is decreasing, its magnitude changes from the outward to the inward direction, and at a certain intermediate radial position, the axial velocity, V_z, becomes zero. It may be observed that at that point, the rate of change of axial velocity in the radial direction, $\partial V_z/\partial r$, is at its maximum. Since shear force is directly proportional to the velocity gradient, the axial shear stress will also approach its maximum in the vicinity of the point where $V_z = 0$.

The tangential momentum imparted to the total flow remains constant at constant control flow rate, and the intensity of swirl will not vary significantly even with different supply flow rates. Experimental results indicated also that the area in which reverse flow occurs decreases slightly as supply flow rate increases for constant control flow rate conditions. This may be due to the fact that all the exhaust flow has to be discharged through the annular region. There are only three possibilities: either the positive axial velocity is increased; or the discharge annular area is increased, or both. Since the true increase in the axial velocity is not as high as that of the total flow rate, the annular flow area must be increased in order that all the flow be discharged to maintain steady flow conditions. The increase in annular discharge area causes, of course, a corresponding reduction in the reverse flow area.

It should be noted, too, that the negative axial velocity component in the reverse flow region is quite constant and independent of the supply flow rate. Its magnitude, therefore, should depend on the tangential momentum since flow in the reverse region is caused by the low pressure generated by the increase in tangential velocity near the core. If the initial tangential flow is the same, the reverse axial velocity component should also remain the same. Results in Figs. 6b, 7b and 8b support this argument.

It can also be seen from the figures that the negative (inward) axial velocity component is not affected by changes in the positive (outward) flow rate. In all these experiments, integration of the axial flow velocity was carried out across the exhaust port area in order to check the continuity between the inlet and exhaust flow. Detailed procedures and results are presented in Appendix II.

3.2.2 The 1.5 inch diameter cylindrical exhaust port

The discussion described in the last section applies to this 1.5 inch diameter case as well. Although the experimental results shown in Figs. 9b, 10b and 11b are slightly different in magnitude, the general trends exhibited by the results are practically identical.

The magnitude of the positive or outward axial velocity for the 1.5 inch diameter case is higher than that for the 2 inch diameter case at the same supply rate. This is simply because the same flow rate has to go through a smaller annular cross-sectional area, therefore, the axial velocity is increased.

It should be noted that the magnitude of the reversed flow rates is also increased. As a result of the decreasing exhaust port diameter, and the conservation of tangential momentum, the increase in tangential velocity for the 1.5 inch diameter exhaust port configuration is much higher than that of the 2 inch diameter case. The increase in tangential velocity results in an even more rapid decrease of static pressure which induces stronger reverse flow.

For constant control flow rate, the reversed flow area decreased when supply flow rate was increased. The explanation for this is the same as as that given in the previous section.

3.2.3 The 30°, 3.6 inch outlet diameter conical exhaust port

The axial velocity and the magnitude of the reverse flow rate for the case shown in Figs. 12b, 13b and 14b are smaller than both the previous cases under the same supply and control flow rates. The reverse flow area, however, is significantly increased. First, the reduction of outward axial velocity component may be explained as follows: The centrifugal force keeps the flow near the wall of the conical exhaust port. In other words, the exit area increases as the flow spiralling out of the conical section. Therefore, the magnitude of the axial velocity is substantially decreased.

As shown by the experimental results, the point at which the axial velocity is zero is much closer to the wall than in the two previous cases. Furthermore, the points are actually closer for the wall for cases of lower supply flow rate. The physical explanation of this phenomenon is exactly the same as that given previously and the effect is further accentuated due to the diverging configuration of the exhaust port.

It is also noted that the slope of the outward axial velocity versus radial position curve becomes steeper as the control flow rate increases. This is due to the increase in tangential velocity causing the severe drop in static pressure which reduces reverse flow.

3.3 Radial Distribution of Tangential Velocity Component

3.3.1 The 2 inch diameter cylindrical exhaust port

Under the flow condition of a supply flow rate of 30 scfm and control flow rates of 10, 15 and 20 scfm, the radial velocity distributions of the exhaust hole are shown in Fig. 11c. The experimental curves indicate that, as the control flow rate is increased, a corresponding increase in the tangential velocity is realized. Hence, the magnitude of tangential components is wholely dependent upon the input control jets.

The magnitude of the tangential velocity initially decreases very rapidly until it reaches the region where axial reverse flow starts when the rate of change is drastically reduced as the flow moves towards the centre. It is also shown in this curve that the swirl never reverses its direction and is always in the same direction as the control input flow.

The axial reverse flow, which is being sucked into the vortex core region, has no angular momentum initially. Its total momentum is imparted to it by the friction of primary exhaust flow through complex momentum exchange mechanisms. Therefore, the maximum tangential velocity gradient ($\partial V_\phi / \partial r$) occurs in the region where axial reverse flow starts (i.e. where $V_z = 0$). In other words, this is the point where maximum transfer of tangential momentum is taking place. Experimental results confirm this finding. Since the reverse flow which is being sucked into the core of the vortex has no initial momentum and all its tangential momentum is imparted to it by the exhaust flow, it is therefore reasonable to expect that the vortex motion in the core region resembles that of a solid body rotation as also shown from the experimental data.

The fact that maximum shear stress occurs in, or near, the region where axial reverse flow starts is of real practical significance. For example, in order to minimize the losses in practical devices where strong vortex motion is utilized, it may be desirable to eliminate, partially or completely, the reverse flow phenomenon. For example, a solid cylinder or cone with diameter approximating that of the reverse flow area may be incorporated into the core region of a vortex chamber. This presents a very interesting subject for future investigation.

It may be of interest to compare various cases with varied supply flow and constant control flow. The results verify the previous work of Wei (16), and Kwok and Lin (17).

A high maximum tangential velocity corresponds to a high supply flow, Qs. If complete mixing of the control and supply flow occurs within the exhaust port, the tangential momentum of the control flow must be totally imparted to the main flow. Increasing the total flow rate therefore causes a reduction in the rate of angular momentum loss, for constant control flow rate, since friction losses depend both on velocity gradient and viscosity.

Friction losses depend on the contact surface area times the maximum shear stress which occurs at the point of zero axial velocity. As flow rate increases, the point of zero axial velocity moves inward leaving a smaller area for the shear stress to act on. Thus, as shown in the experimental results, a larger total flow rate gives lower friction losses and a smaller reverse axial flow area.

These factors are marginal but additive and correspond to the difference in radial distribution of the tangential velocity shown in Figs. 6c, 7c and 8c.

3.3.2 The 1.5 inch diameter cylindrical exhaust port

The experimental results for the case of a 1.5 inch diameter exhaust port (shown in Figs. 9c, 10c and 11c) are very similar to those of the 2 inch diameter case, except for the fact that the tangential velocity in this case is slightly higher. This can be explained simply by the concept of conservation of tangential momentum. When the exhaust hole diameter is reduced, the maximum tangential velocity attained is also expected to increase.

The maximum shear stress occurs also very close to the point where the reverse flow starts and the core of the reverse flow region exhibits solid body rotation with a gradual decrease of tangential velocity near the centre.

3.3.3 The 30°, 3.6 inch outlet diameter conical exhaust port

These experiments were performed under the same conditions as those in the two previous cases with cylindrical exhaust ports; however, the results are quite different.

The tangential velocity is zero at the wall. It increases rapidly to a maximum at the non-dimensionalized radial position of approximately 0.8 and then tapers gently back to zero at the centre of the port. Notice that the maximum tangential velocity here is much lower than those in the preceding cases. The centrifugal forces make the exit flow adhere to the wall of the exhaust port. By conservation of angular momentum, as the radius of the swirl flow increases, the tangential velocity decreases correspondingly.

With the diverging cone exhaust port configuration, all the positive axial flow leaves the chamber within a fairly thin annular region. As a result, the reverse flow occupies most of the exhaust port region. Solid body rotation of the reversed flow is especially evident in this set of experimental results.

3.4 Radial Distribution of Radial Velocity Component

The sign convention used for radial flow in this dissertation corresponds to that of Wei (17), that is, inward flow is positive.

3.4.1 The 2 inch diameter cylindrical exhaust port

Experimental results of the radial velocity distribution are shown in Figs. 6a, 7a and 8a. The spiralling flow from the exhaust port resembles flow along concave walls. Stationary Taylor-Görtler rings rotating about a helical axis along the spiral path were caused by the destabilizing centrifugal forces. The Taylor-Görtler rings are superimposed on the main flow. A ring is expected between the wall and the first point of zero radial velocity; however, the limited data obtained in this region are not adequate to confirm its presence.

A second ring is induced by the first, occurring between the first and second points of zero radial velocity and rotating in the opposite direction to the first.

The Taylor-Görtler vortices reported by Wei (17) were confirmed:

> "The most significant discovery from the experimental data is that the radial velocity distributions reveal the existence of complex Taylor-Görtler vortices. According to the flow described above, the resultant radial velocity distribution must approach that of a sine wave. In order to clearly understand this phenomenon, it may be instructive to consider the projected linear velocity of a point moving around a circular path as in simple harmonic motion. The magnitude of the velocity of the point when it is projected onto the plane perpendicular to the path must necessarily resemble that of a sine wave. In the present case, the flow may be visualized using this highly simplified model, although the actual flow is more complex due to the superposition of a main spiral outward flow. Nevertheless, the results in Figs. 6a, 7a and 8a clearly indicate such a trend and substantiate the interpretation of the flow model."

A third vortex ring is induced opposing the second ring and occurring in the region between the edge of the second ring (where $V_r = 0$) and the centre of the channel. The direction of the rotation of the three rings is such that the tangential velocities at adjacent sides of adjacent rings are in the same direction so that the rotation of adjacent rings is always in opposite directions. The direction of rotation can be determined in experimental data from positive or negative variations in the radial velocity distribution.

The results described in this dissertation are different from those obtained by Wei (16), and Kwok and Lin (17). In the present work, only three vortex rings were observed, while in references (16) and (17), four vortex rings were described. It was found that an error was involved in the calculation of the experimental data presented in references (16) and (17), and the fourth vortex ring described was in fact not present.

3.4.2 The 1.5 inch diameter cylindrical exhaust port

The experimental results shown in Figs. 9a, 10a and 11a are similar to those described in the preceding section. As the radius of the port decreases, the outward radial velocity increased. As a result, the intensity of the vortex ring nearest the wall is also significantly increased. As in the previous case, three counter-rotating vortex rings were observed.

Comparing the radial velocity component for the cases of the 2 inch and 1.5 inch diameter exhaust ports, it can be seen that the mangitude of the radial velocity for the latter case is slightly higher. The total flow rate

$$Q = (2\pi rh)V_r \qquad (3.4.2\text{-}1)$$

As r is reduced from 2 to 1.5 inch, for constant flow rate, V_r is expected to increase correspondingly. In general, the intensity of the Taylor-Görtler type vortex for the 1.5 inch diameter exhaust port is stronger than that of the 2 inch diameter exhaust port.

The experimental results also exhibit a gradual decrease in the radial velocity component with constant supply flow rate, Q_s, and decreasing control flow rate, Q_c. According to equation (3.4.2-1), V_r will also decrease for decreasing control flow rate.

3.4.3 The 30°, 3.6 inch outlet diameter conical exhaust port

The results shown in Figs. 12a, 13a and 14a are basically similar to those in the previous two cases. Due to the conical shape of the exhaust port, the centrifugal force keeps the flow along the diverging wall of the conical exhaust port. Using equation (3.4.2-1), as r is increased, V_r will decrease correspondingly. This is why the intensity of the Taylor-Görtler vortex for this type of conical exhaust port is relatively weak. It is also evident that the third ring closest to the centre is particularly weak.

The relatively large reverse flow area coupled with the low intensity of the second vortex ring accounts for this observation.

3.5 Radial Distribution of Wall Static Pressure

Static pressures measured at various radial locations in the annulus of the vortex chamber are shown in Figs. 15 to 17. Predictably, high static pressure corresponds to high control flow rate, since additional pressure is needed to induce flow into the vortex chamber.

The static pressure gradient along a radial line increases with increased control flow rate. Too, the tangential velocity in the chamber and hence the friction loss increases with increased control flow. The drop in static wall pressure indicates an increase in the usual and tangential velocities as can be predicted from the principles of conservation of angular momentum and continuity.

For a smaller exhaust port, the static pressure should be higher for the same flow rate. This is evident since more pressure is required to force the same amount of flow through a smaller orifice. However, it is expected that the static pressure drop will be higher for the case with smaller exhaust port diameter. This is due to the substantial increase in both the tangential and radial velocity components. The decrease in wall static pressure, a function of the square of the velocity vector, increases near the exhaust where both the tangential and radial velocity components increase.

The data obtained using various control flow rates with fixed supply flow are shown in Figs. 15, 16 and 17. The marked sensitivity of static pressure to control flow rate, which is evident in these data, is utilized in vortex amplifiers to produce a high turn down ratio since a small change in control flow causes a large increase in pressure in the chamber, preventing flow into the chamber. Thus, a high pressure control signal, even at a very low flow rate, can be used to control a much larger supply flow.

CHAPTER 4

CONCLUSIONS

A 10 inch vortex chamber was built for the experimental investigation of the exhaust flow velocity profile. The chamber was designed to allow investigation of various exhaust port diameters, input velocity ratios, and chamber heights.

Detailed measurements of the exit velocity profiles indicate the following:

a) A strong axial reverse flow region exists in the vortex core region under high swirl conditions. The reverse flow area is strongly dependent on the the total input tangential momentum.

b) The existence of the Taylor-Görtler vortices is demonstrated by the radial distribution of radial velocity components. The present results indicate that a total of three counter-rotating vortex rings exists for exhaust ports with cylindrical or conical configurations. In each case, the two outer vortex rings move in an outward direction while the inner one moves in the opposite direction.

c) The experimental results of the velocity distribution at the exit plane of the exhaust flow provide a good understanding of the complex flow mechanism.

Regions where maximum shear stress occur revealed important information for engineers designing practical devices utilizing the vortex phenomenon.

CHAPTER 5

RECOMMENDATIONS FOR FUTURE STUDIES

Future work should be carried out by investigating the effect of vortex chamber aspect ratios on the velocity profiles under various supply and control flow conditions. In order to improve symmetry of the vortex flow, it will be necessary to increase the number of tangential nozzles in the vortex chamber.

Too, it would be interesting to place small solid bodies of different shapes inside the exhaust port to investigate the effect of the introduction of the solid body on flow and velocity distributions.

REFERENCES

1. Rott, N., "On the Viscous Core of a Line Vortex", ZAMP, vol. IXb, 1958, p. 543. "Turbulent Boundary Layer Development on the End Walls of a Vortex Chamber", Aerospace Corp., Report ATN-62(9202)-1, 1962.

2. Donaldson, C. du P. and Sullivan, R.D., "Examination of the Solutions of the Navier-Stokes Equations for a Class of Three-Dimensional Vortices", Zero Research Associates of Princeton AFOSR, TN60-1277, Oct. 1960.

3. Kendall, J.M. Jr., "Experimental Study of Turbulence in a Driven Vortex", Tech. Report No. 32-290, Jet Propulsion Laboratory, California Institute of Technology, June 1962.

4. Kwok, C.K., "Vortex Flow in a Thin Cylindrical Chamber and Its Application in Fluid Amplifier Technology", Ph.D. Thesis, McGill University, Montreal, 1966.

5. Savino, Joseph M. and Ragsdale, Robert G., "Some Temperature and Pressure Measurements in Confined Vortex Fields", J. Heat Transfer (Trans. ASME), series C, vol. 83, No. 1, Feb. 1961.

6. Beverloo, W.A., Leniger, H.A. and Weldring, J.A.G., "Potentialities of the Flat Vortex 'Hydrosifter'", Brit. Chem. Eng. J., vol. 8, No. 10, Oct. 1963.

7. Kerrebrock, J.L. and Meghreblian, R.V., "An Analysis of Vortex Tubes for Combined Gas-Phase Fission Heating and Separation of the Fissionable Material", ONRL-CF-47-11-3, 1957.

8. Donaldson, C. du P., "The Magnetohydrodynamic Vortex Power Generator", Basic Principles and Practical Problems: Aeronautical Associates of Princeton, Report No. 30, March 1961.

9. Willison, G.G. and McCune, J.E., "A Preliminary Study of the Structure of Turbulent Vortices", Aeronautical Associates of Princeton, Report No. 32, July 1961.

10. Williamson, Guy G. and Donaldson, C. du P., "An Experimental Study of Turbulence in a Driven Vortex", Aeronautical Research Associates of Princeton, Report No. ARAP TM-64-2, July 1964.

11. King, W.S., "Momentum Integral Solutions for the Laminar

Boundary Layer on a Finite Disk in a Rotating Flow", Aerospace Corp., Report ATN-63(9227)-3, 1963.

12. Weber, H.E., "Boundary Layer Inside a Conical Surface Due to Swirl", J. of Applied Mechanics, vol. 23, Trans. ASME, vol. 78, 1956.

13. Ostrach, S. and Loper, D.E., "An Analysis of Confined Vortex Flows", AIAA paper No. 66-88, 1966.

14. Wormley, D.N., "An Analytical Model for the Incompressible Flow in Short Vortex Chambers", J. of Basic Engineering, Trans. ASME, series D, vol. 92, No. 2, June 1969, p. 264.

15. Thinh, N.D., "An Analytical Investigation of Confined Vortex Flow Phenomena", J. of Basic Engineering, Sept. 1972.

16. Wei, B.M., "An Experimental Investigation of Confined Vortex Phenomena", Master's Dissertation, Sir George Williams University, Montreal, June 1971.

17. Kwok, C.K. and Lin, S., "Some Observations of Vortex Flow Phenomena", Fourth Canadian Congress of Applied Mechanics, Montreal, May 1973.

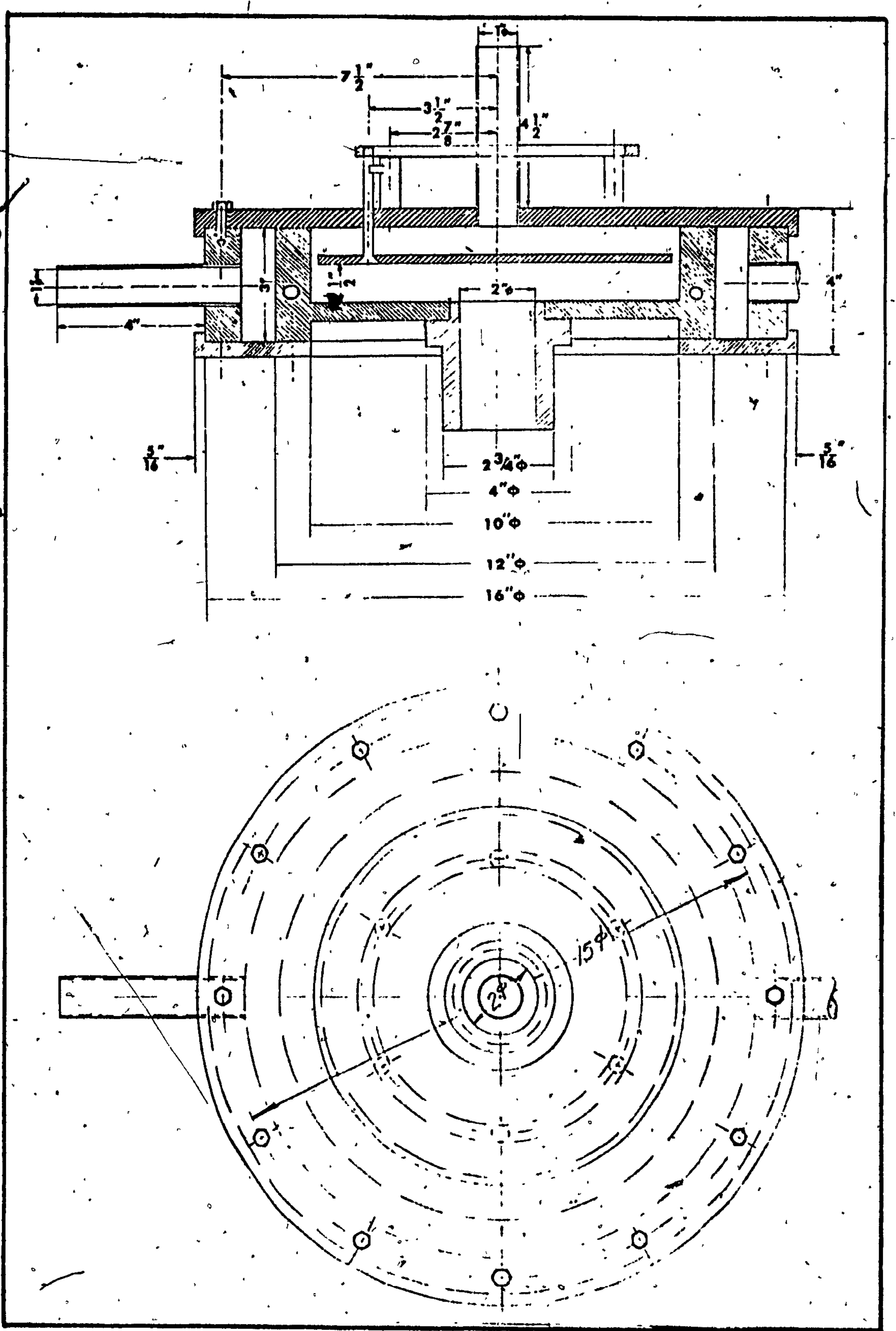

FIG.1 EXPERIMENTAL VORTEX CHAMBER

FIG. 2 THREE DIFFERENT SIZES OF EXHAUST PORT

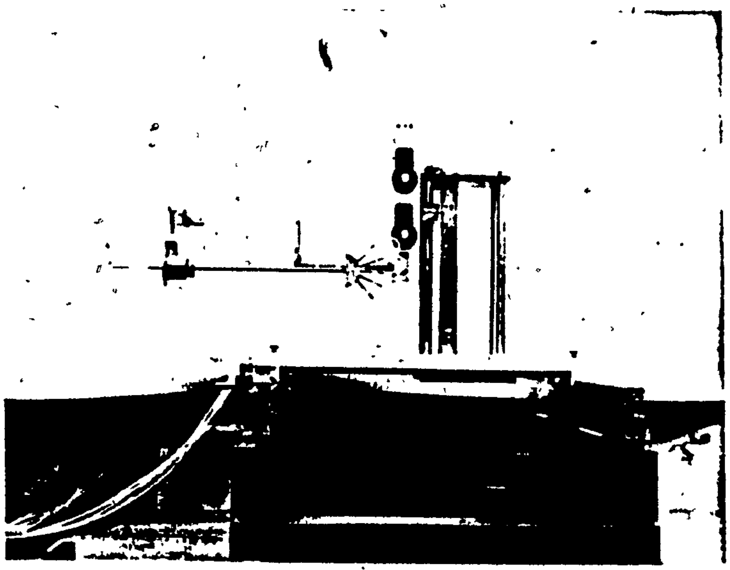

FIG. 3 TRAVERSING MECHANISM

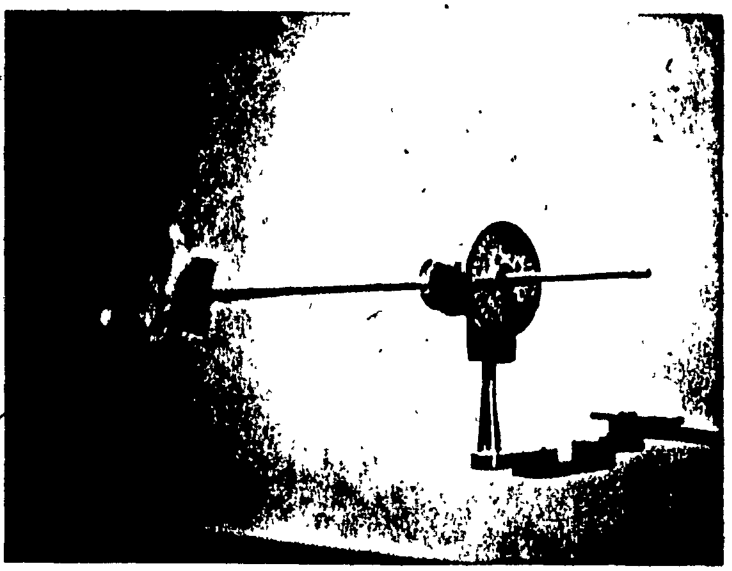

FIG. 4 5-HOLE DIRECTION PROBE

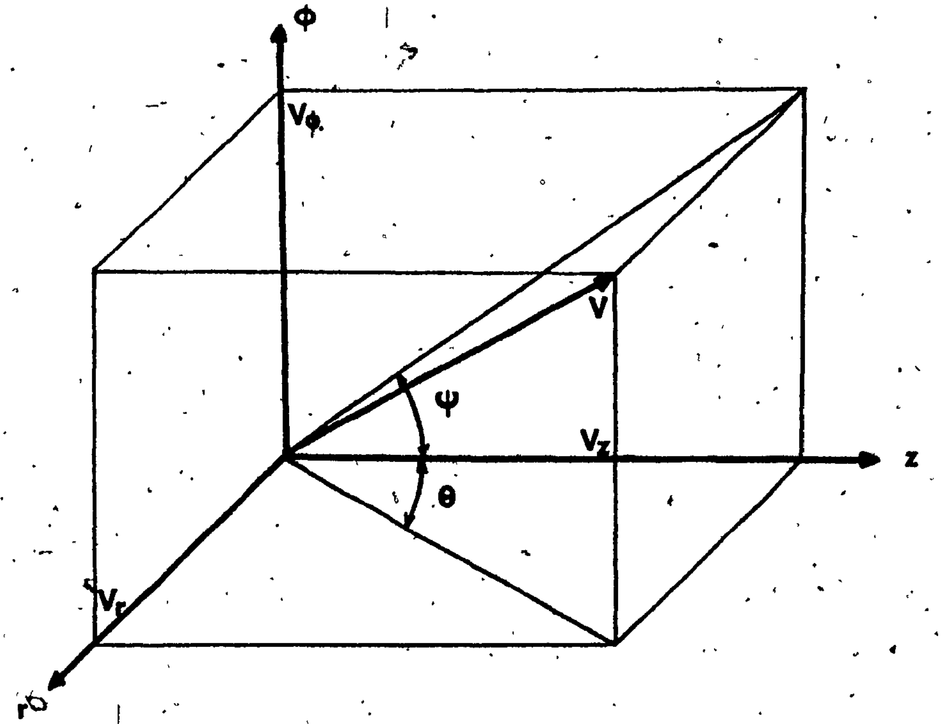

FIG. 5 VELOCITYVECTOR IN CYLINDRICAL COORDINATE

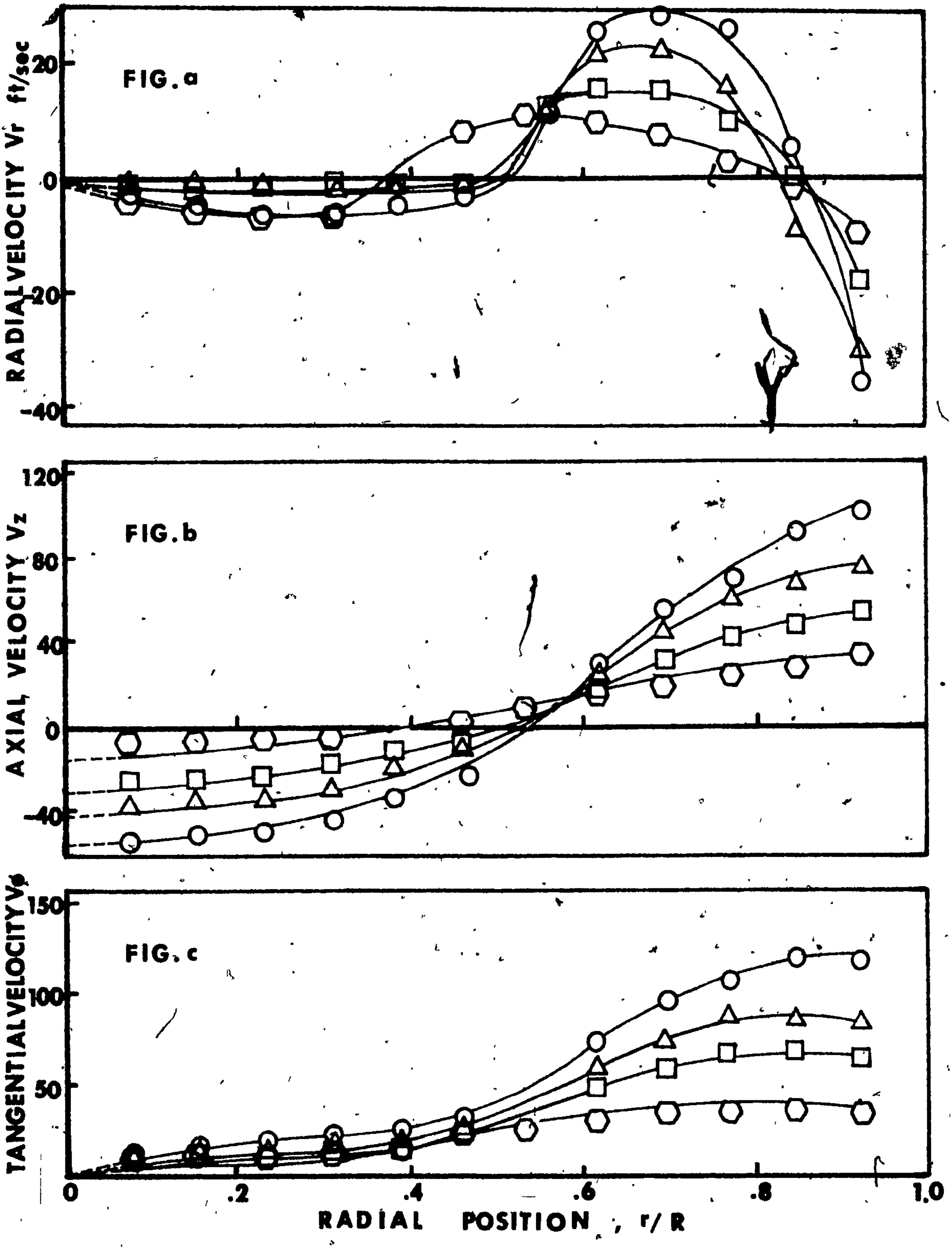

FIG.6 RADIAL DISTRIBUTION OF VELOCITIES.

Dex = 2 in, ○ , Q_s = 10 scfm , Q_c = 20 scfm .
△ , Q_s = 10 scfm , Q_c = 15 scfm .
□ , Q_s = 10 scfm , Q_c = 10 scfm .
⬡ , Q_s = 10 scfm , Q_c = 5 scfm .

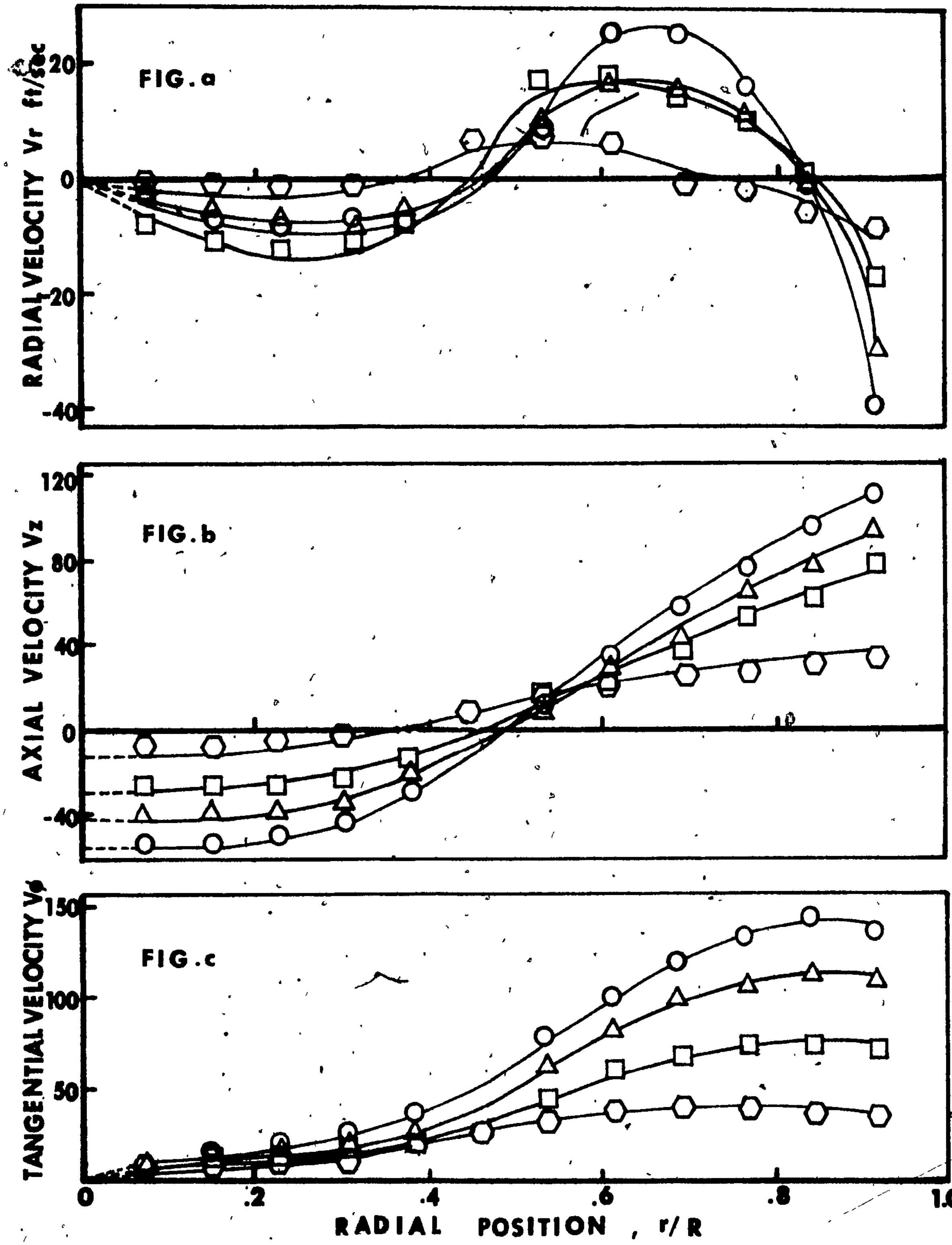

FIG.7 RADIAL DISTRIBUTION OF VELOCITIES.

D_{ex} = 2 in. ○ , Q_s = 20 scfm , Q_c = 20 scfm .
△ , Q_s = 20 scfm , Q_c = 15 scfm .
□ , Q_s = 20 scfm , Q_c = 10 scfm .
⬡ , Q_s = 20 scfm , Q_c = 5 scfm .

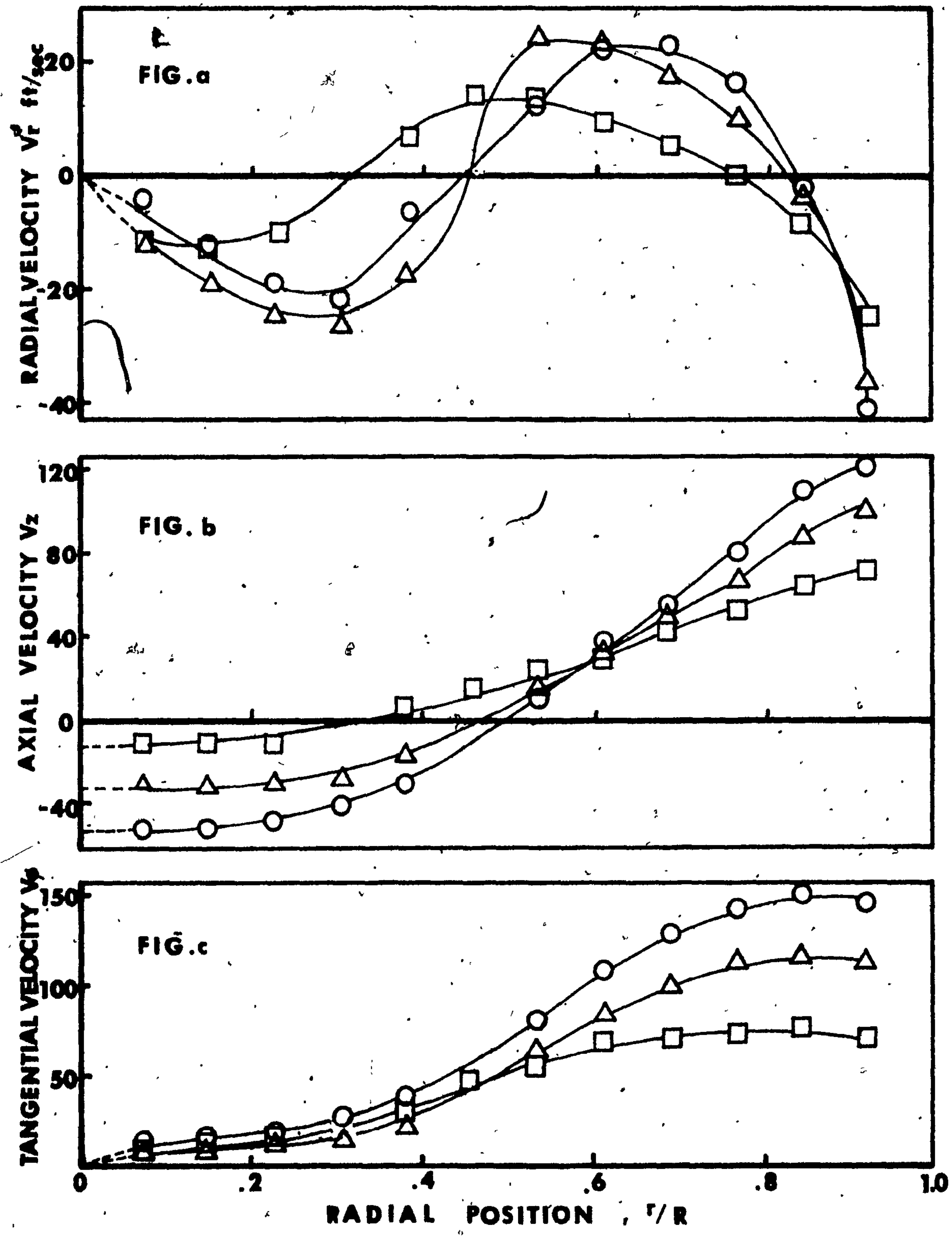

FIG. 8 RADIAL DISTRIBUTION OF VELOCITIES.

D_{ex} = 2 in., ○ , Q_s = 30 scfm , Q_c = 20 scfm .
△ , Q_s = 30 scfm , Q_c = 15 scfm .
□ , Q_s = 30 scfm , Q_c = 10 scfm .

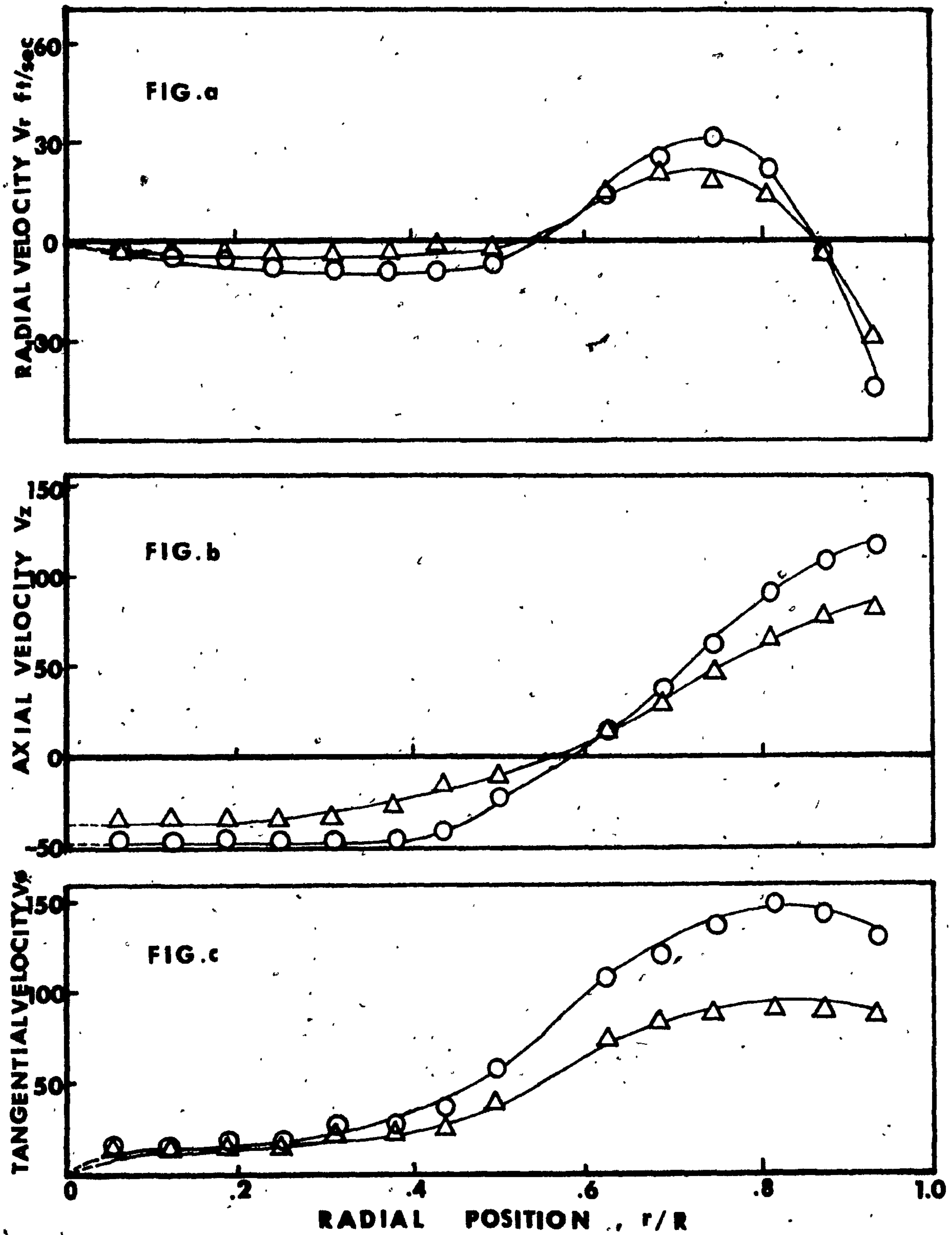

FIG. 9 RADIAL DISTRIBUTION OF VELOCITIES.

Dex = 1.5 in. ○, Q_s = 10 scfm, Q_c = 15 scfm.

△, Q_s = 10 scfm, Q_c = 10 scfm.

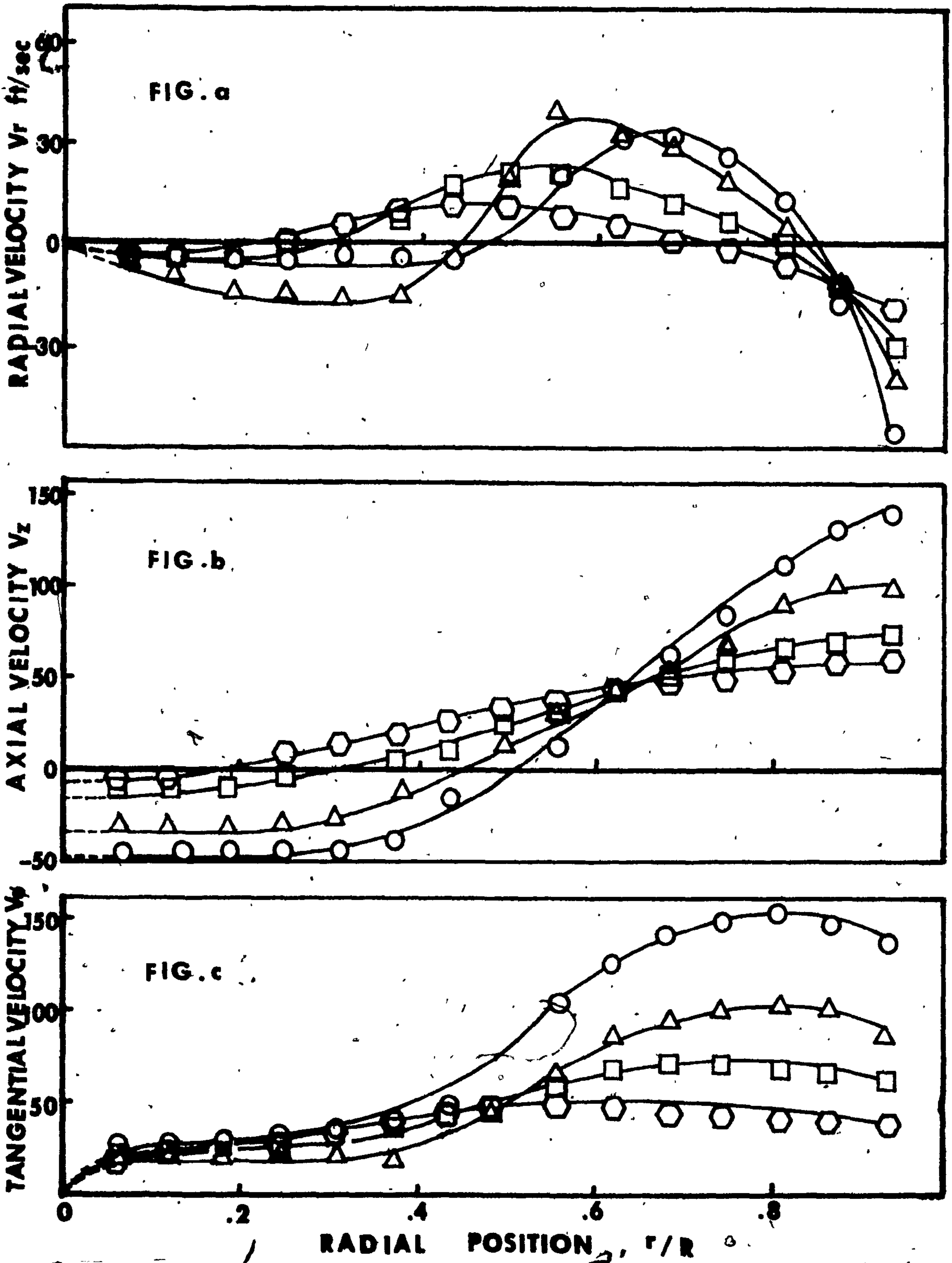

FIG.10 RADIAL DISTRIBUTION OF VELOCITIES.

Dex=1.5 in. ○ , Q_s = 20 scfm , Q_c = 15 scfm
△ , Q_s = 20 scfm , Q_c = 10 scfm
□ , Q_s = 20 scfm , Q_c = 7 scfm
⬡ , Q_s = 20 scfm , Q_c = 5 scfm

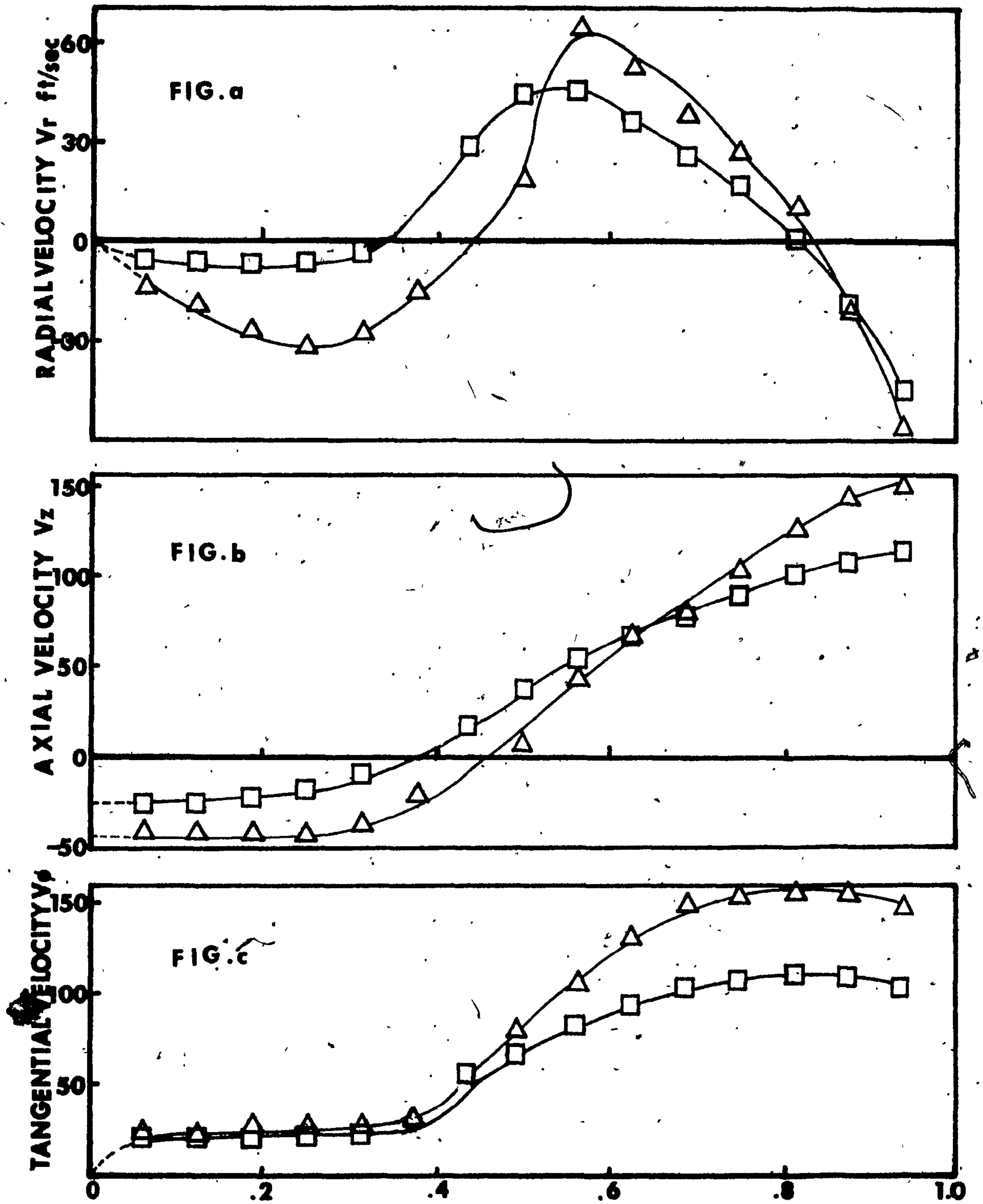

FIG.11 RADIAL DISTRIBUTION OF VELOCITIES.

Dex = 1.5in. △ , Q_s = 30 scfm , Q_c = 15 scfm .
□ , Q_s = 30 scfm , Q_c = 10 scfm .

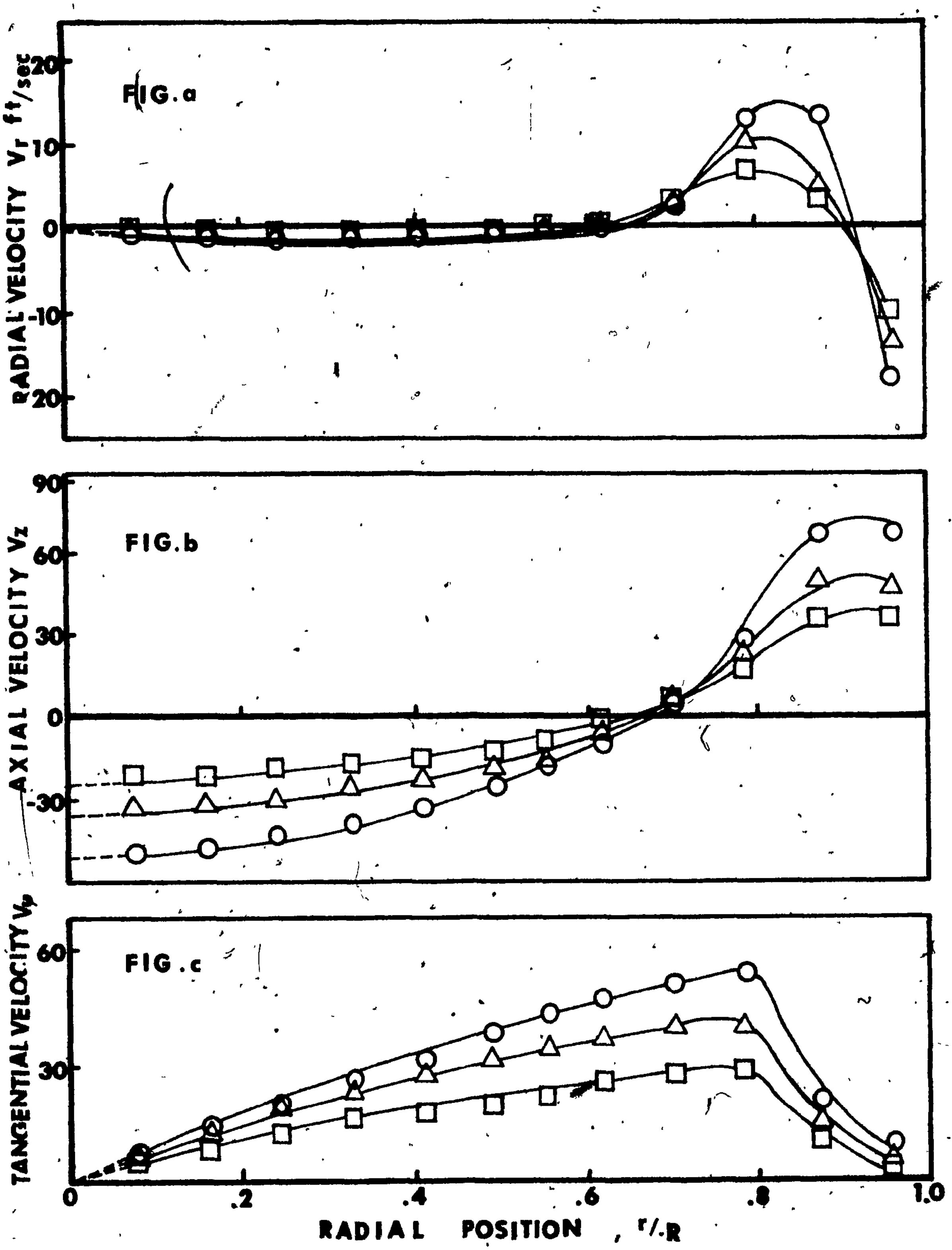

FIG.12 RADIAL DISTRIBUTION OF VELOCITIES.

D_{ex} = 3.6 in. ○ , Q = 10 scfm , Q_c = 20 scfm.
△ , Q = 10 scfm , Q_c = 15 scfm.
□ , Q = 10 scfm , Q_c = 10 scfm.

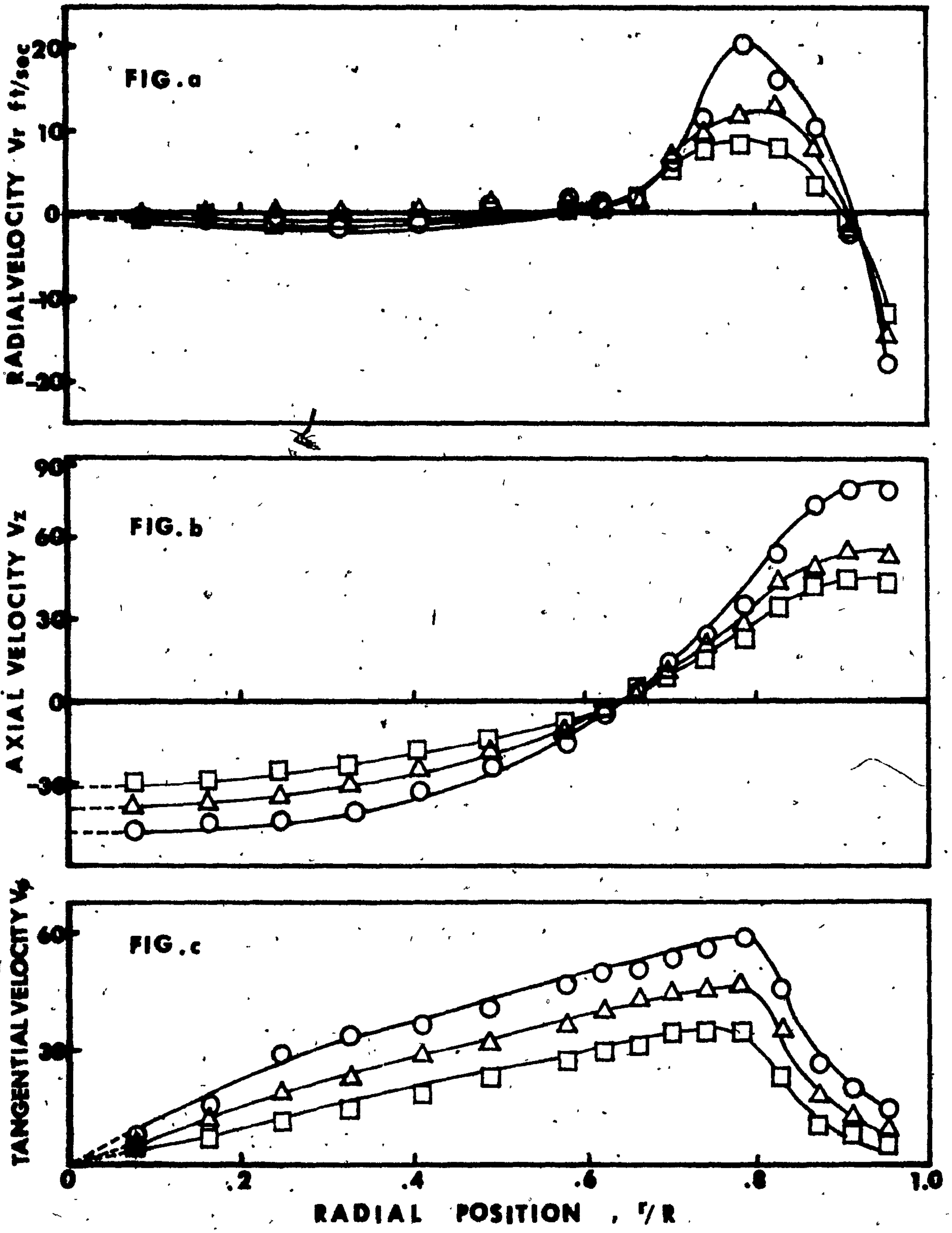

FIG.13 RADIAL DISTRIBUTION OF VELOCITIES.

$D_{ex} = 3.6$ in. ○ , $Q_s = 20$ scfm , $Q_c = 20$ scfm.
△ , $Q_s = 20$ scfm , $Q_c = 15$ scfm.
□ , $Q_s = 20$ scfm , $Q_c = 10$ scfm.

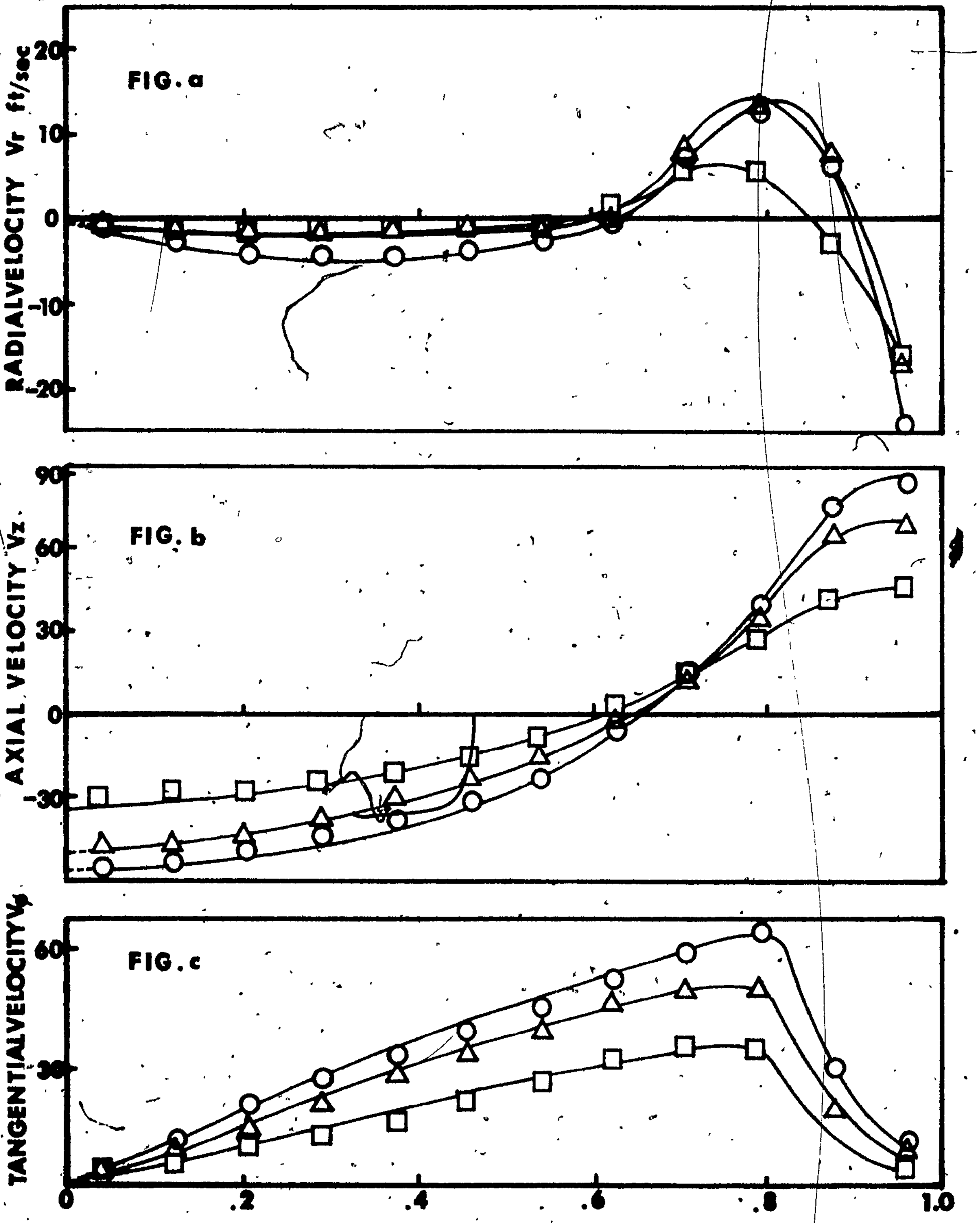

FIG. 14 RADIAL DISTRIBUTION OF VELOCITIES.

D_{ex} = 3.6 in. ○ , Q_s = 30 scfm , Q_c = 20 scfm .
△ , Q_s = 30 scfm , Q_c = 15 scfm .
□ , Q = 30 scfm , Q_c = 10 scfm .

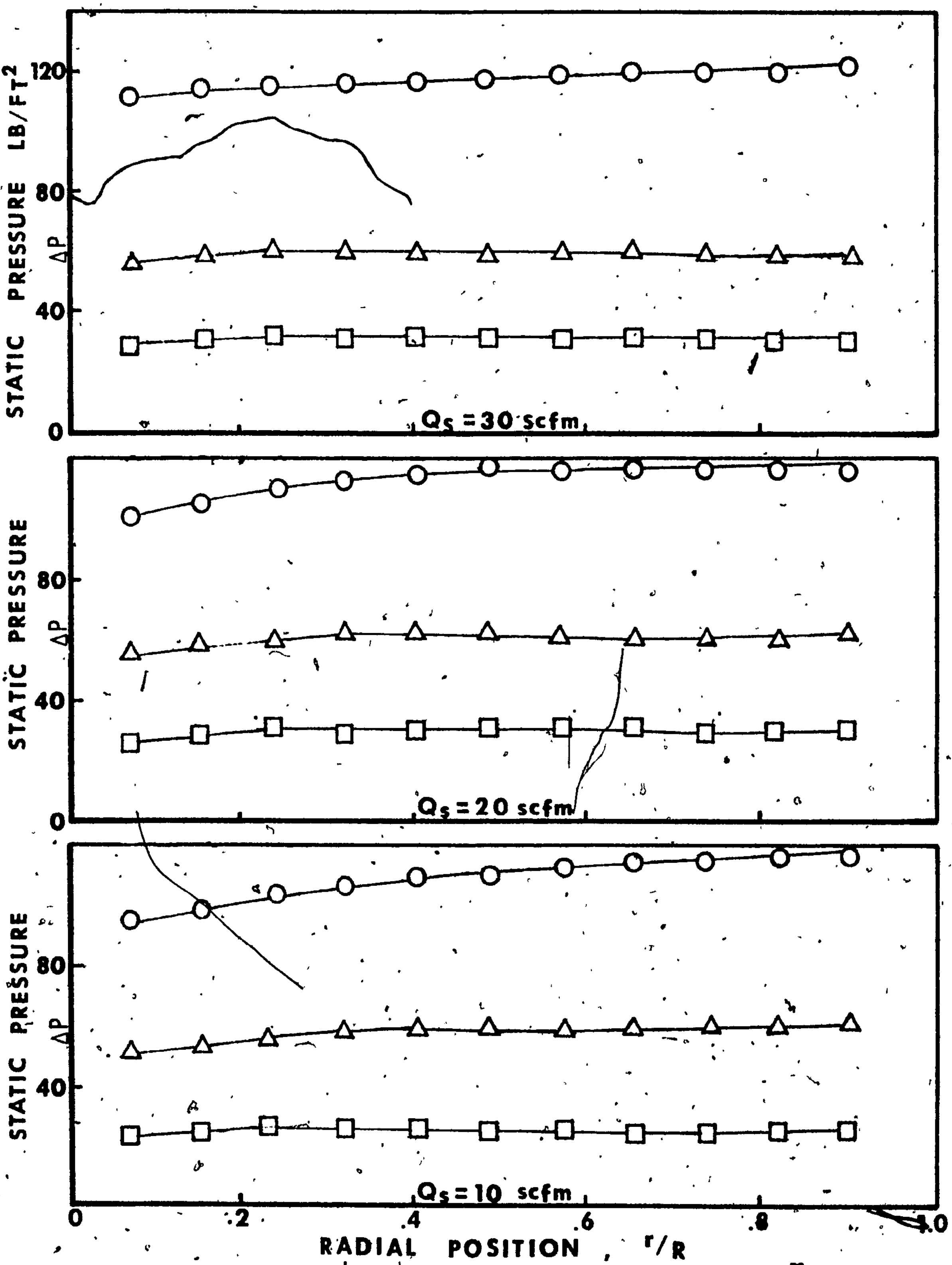

FIG. 15 STATIC PRESSURE DISTRIBUTION IN 10"-DIA. CHAMBER Dex = 2 in.

○ , Q_c = 20 scfm.
△ , Q_c = 15 scfm.
□ , Q_c = 10 scfm.

ΔP = static pressure-ambient pressure

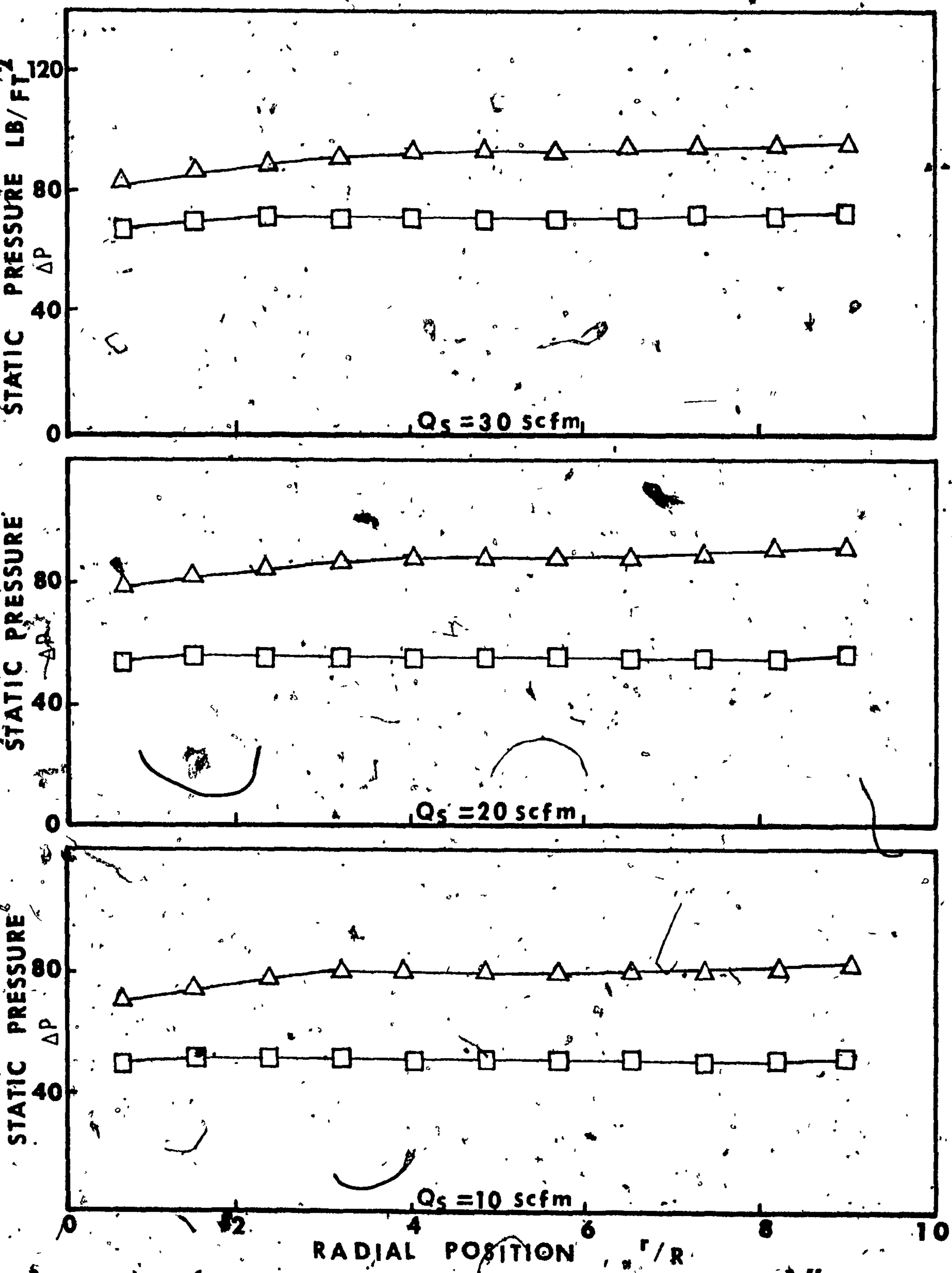

FIG. 16 STATIC PRESSURE DISTRIBUTION IN 10"-DIA. CHAMBER $D_{ex} = 1.5$ in. △ , $Q_c = 15$ scfm.
□ , $Q_c = 10$ scfm.
ΔP = static pressure-ambient pressure

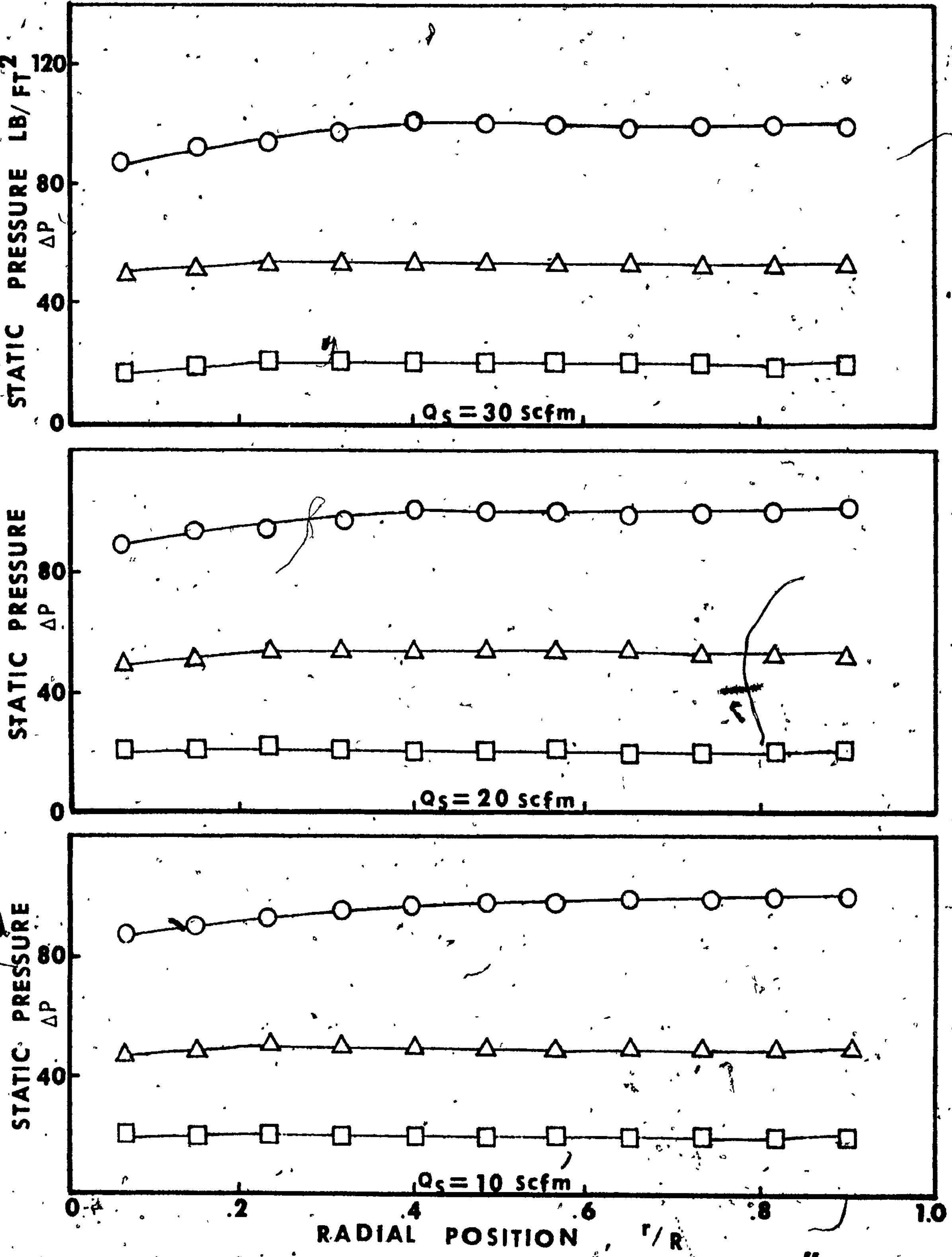

FIG.17 STATIC PRESSURE DISTRIBUTION IN 10"-DIA. CHAMBER Dex = 3.6 in.

○ , Q_c = 20 scfm .
△ , Q_c = 15 scfm .
□ , Q_c = 10 scfm .

ΔP = static pressure-ambient pressure

APPENDIX I

DATA REDUCTION

From the energy equation:

$$P_t - P_{s1} = \rho V^2/2$$

$$V = SQRT(2(P_t - P_{s1})/\rho)$$

where $\rho = 0.002378$ slug/ft^3

Fig. 5 shows diagrammatically that the velocity vector can be resolved into tangential, radial and axial components by the following procession:

$$V^2 = V_r{}^2 + V_\phi{}^2 + V_z{}^2 \quad (1)$$

$$V_{rz}{}^2 = V_r{}^2 + V_z{}^2 = V_r{}^2/\sin^2\theta \quad (2)$$

$$V_{\phi z}{}^2 = V_\phi{}^2 + V_z{}^2 = V_\phi{}^2/\sin^2\psi \quad (3)$$

from eq. (2)

$$V_z{}^2 = V_r{}^2(1/\sin^2\theta - 1) \quad (4)$$

from eq. (3)

$$V_z{}^2 = V_\phi{}^2(1/\sin^2\psi - 1). \quad (5)$$

eq. (4) = eq. (5)

$$V_\phi{}^2 = V_r{}^2((1/\sin^2\theta - 1)/(1/\sin^2\psi - 1)) \quad (6)$$

eq. (4) and eq. (6) into eq. (1).

$$V^2 = V_r{}^2 + ((1/\sin^2\theta-1)/(1/\sin^2\psi-1))V_r{}^2 + (1/\sin^2\theta-1)V_r{}^2$$

$$\therefore V_r{}^2=V^2(\sin^2\theta(1-\sin^2\psi)/(1-\sin^2\theta\cdot\sin^2\psi))$$

$$V_r = V\sin\theta\cdot\cos\psi/\mathrm{sqrt}\cdot(1-\sin^2\theta\cdot\sin^2\psi)$$

$$\therefore V_\phi{}^2=V^2(\sin^2\psi(1-\sin^2\theta)/(1-\sin^2\theta\cdot\sin^2\psi))$$

$$V_\phi = V\sin\psi\cdot\cos\theta/\mathrm{sqrt}\cdot(1-\sin^2\theta\sin\psi)$$

$$\therefore V_z{}^2 = (1/\sin^2\theta-1)V_r{}^2=V^2(1-\sin^2\theta(1-\sin^2\psi)/(1-\sin^2\theta\cdot\sin^2\psi)$$

$$V_z = V\cos\theta\cdot\cos\psi/\mathrm{sqrt}\cdot(1-\sin^2\theta\cdot\sin^2\psi)$$

APPENDIX II

ANALYSIS BY THE CONTINUITY EQUATION

For estimating the accuracy of the experimental result, the flow rate from the exhaust port, Q, was calculated from the velocity component in the axial direction determined by the experimental data in comparison with the supply flow rate, Q_s, plus the control flow rate, Q_c. A difference method was used to calculate the flow rate from the exhaust port; this is shown in Fig. 1. The deviation of the measurement calculated is shown in Table 1, and is defined as follows:

$$\varepsilon = \frac{(Q_s + Q_c) - Q}{Q_s + Q_c} \times 100\%$$

From Table 1, it is seen that the maximum deviation of the measurement is ± 30%.

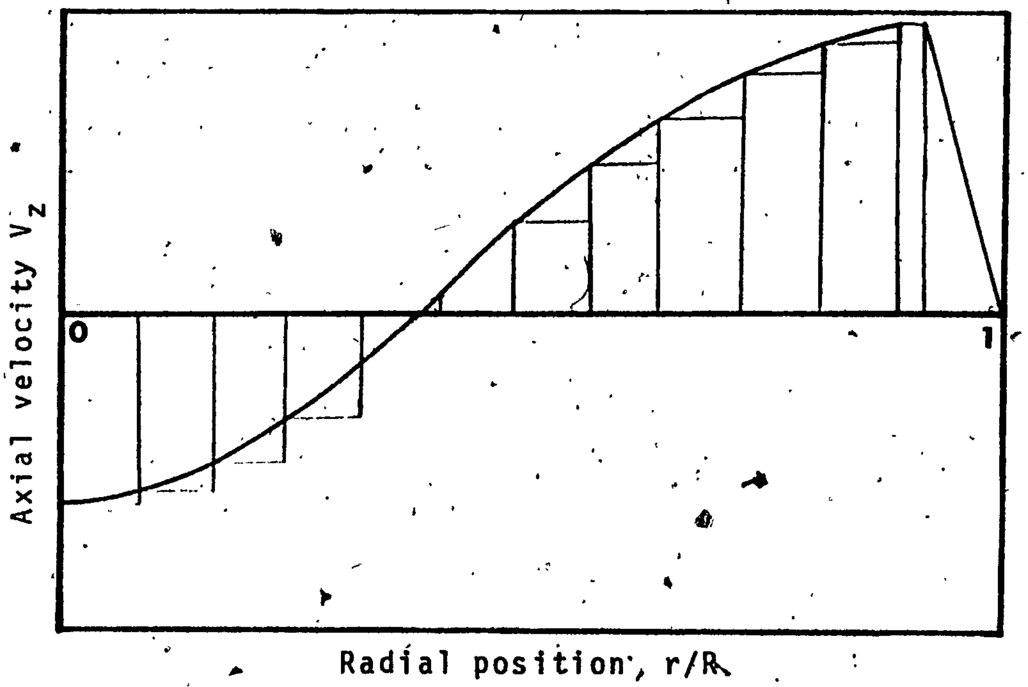

Fig. 1 Calculation of flow rate from exhaust port

TABLE 1 Percentage Deviation

Error % Flow Rate		1.5 in.	2.0 in.	3.6 in.
Q_c = 20 scfm	Q_s = 30 scfm		-5.0	-17.0
	Q_s = 20 scfm		12.0	8.0
	Q_s = 10 scfm		25.0	-21.0
Q_c = 15 scfm	Q_s = 30 scfm	13.0	0.0	-9.0
	Q_s = 20 scfm	-10.0	5.0	3.0
	Q_s = 10 scfm	-15.0	30.0	1.0
Q_c = 10 scfm	Q_s = 30 scfm	23.0	6.0	-8.0
	Q_s = 20 scfm	3.0	14.0	-7.0
	Q_s = 10 scfm	-6.0	25.0	11.0
Q_c = 5 scfm	Q_s = 30 scfm			
	Q_s = 20 scfm	21.0	-22.0	
	Q_s = 10 scfm		8.0	